Propagating Structural Perturbation Inside Bacteriorhodopsin: Crystal Structures of the M State and the D96A and T46V Mutants†

Janos K. Lanyi* and Brigitte Schobert

Department of Physiology and Biophysics, University of California, Irvine, California 92697

Received June 29, 2006; Revised Manuscript Received August 9, 2006

ABSTRACT: The X-ray diffraction structure of the non-illuminated D96A bacteriorhodopsin mutant reveals structural changes as far away as 15 Å from residue 96, at the retinal, Trp-182, Ala-215, and waters 501, 402, and 401. The Asp-to-Ala side-chain replacement breaks its hydrogen bond with Thr-46, and the resulting separation of the cytoplasmic ends of helices B and C is communicated to the retinal region through a chain of covalent and hydrogen bonds. The unexpected long-range consequences of the D96A mutation include breaking the hydrogen bond between O of Ala-215 and water 501 and the formation of a new hydrogen bond between water molecules 401 and 402 in the extracellular region. Because in the T46V mutant a new water molecule appears at Asp-96 and its hydrogen-bond to Ile-45 replaces Thr-46 as its link to helix B, the separation of helices B and C is smaller than that in D96A, and there are no atomic displacements elsewhere in the protein. Propagation of conformational changes along the chain between the retinal and Thr-46 had been observed earlier in the crystal structures of the D96N and E204Q mutants but in the trapped M state. Consistent with the perturbation of the retinal region in D96A, little change of the Thr-46 region occurs between the non-illuminated and M states of this mutant. It appears that a local perturbation can propagate along a track in both directions between the retinal and the Asp-96/Thr-46 pair, either from photoisomerization of the retinal in the wild-type protein in one case or from the D96A mutation in the other.

Light-driven proton transport in bacteriorhodopsin is dependent on a few key residues, such as Lys-216, Asp-85, and Asp-96, and they have been identified in part from the distinctive phenotypes of mutants in which the replaced amino acids are unable, or much less able, to perform their normal roles (*1*−*3*). Other residues, such as Tyr-185, Glu-194, Glu-204, and Arg-82, play more dispensable roles, as suggested by the altered but less defective phenotypes of their site-specific mutations (*4*−*9*). As usual, such assignments make the assumption that the effects of mutations are local and interpretable in terms of differences in side-chain volume, hydrogen bonding, ability to protonate and deprotonate, and so forth. Of necessity, they ignore the possibility of changes distant from the site of mutation. As often acknowledged, this assumption might not be justified in all cases, and for an unambiguous interpretation of the effects of mutations, structural information about the non-illuminated state as well as the intermediates of the altered reaction cycles would be needed.

How good is the assumption of purely local perturbation in site-specific bacteriorhodopsin mutants? Crystal structures are available for several mutants, and they show that the extent of perturbation depends greatly on the residue that is exchanged, on the residue that replaced it, and on the changing local environment during the photocycle. The V49A mutation causes no structural alteration of the non-illuminated state other than the shorter side-chain (*10*), but the decay of the N state in the photocycle is considerably lengthened, suggesting that there may be greater structural consequences in this intermediate (*11*). The V219L mutation results in a cavity filled with two additional water molecules (*10*) but otherwise little change in the structure, although the N state also has a longer lifetime. The E204Q mutation causes local changes in the positions of water molecules and the position of the nearby Glu-194, but these displacements do not extend far into the protein (*12*). In the D96N mutant, a new water molecule appears (*13*) as far as 7 Å from residue 96. The lifetime of the M and O states of the photocycle are strongly altered in the latter two mutants. Introducing a proline (*14*) causes little change in the structure when near the surface (in K41P) but distorts the main chain when in the middle of a transmembrane helix (in A51P). The greatest global effect is by the D85S mutation, which radically alters the entire structure and results in changed crystal contacts, changed helical tilts, and the redistribution of bound water (*15*).

There is reason to believe that at least some mutations should have more than purely local effects. Point mutations and the photoisomerization of retinal are both structural perturbations at a single, well-defined location. The thermal reactions in the photocycle are the consequences of the rotation of the C_{13}═C_{14} retinal double bond, but eventually they include atomic displacements throughout the protein. If the conformational possibilities available to the protein include only a few stable (or quasi-stable) states, then the global structural changes might be assumed not only

† This work was supported in part by grants to J.K.L. from NIH (R01-GM29498) and DOE (DEFG03-86ER13525).

* Corresponding author. Phone (949) 824-7150. Fax: (949) 824-8540. E-mail: jlanyi@orion.oac.uci.edu.

10.1021/bi061310i CCC: $33.50
Published on Web 09/12/2006

transiently in the functional cycle but also when induced by an appropriate side-chain replacement. In some mutants, this seems to be indeed the case. The outward tilt of helix F that characterizes the late M and N intermediates (*16*−*22*) was observed in the non-illuminated states of D85N at alkaline pH, D85N/D96N at neutral pH (*20*, *23*−*25*), and the D96G/F171C/F219L triple mutant (*17*, *18*). Coupling between the protonation state of Asp-96 and the isomeric state of the retinal was observed not only in the N photointermediate but also in the non-illuminated mutants of Asp-85 (*26*).

One of the long-range effects in the photocycle is the destabilization of the protonated Asp-96 in the cytoplasmic region; therefore, it will become the proton donor to the Schiff base. This article explores, therefore, the stable structural changes caused by the mutation of Asp-96 and its hydrogen-bonding partner Thr-46. The role of this region in proton transport has been described in crystallographic studies (*27*). The creation of a hydrogen-bonded chain of four water molecules in the photochemical cycle begins with the formation of a water cluster at Asp-96. A water molecule intercalates between the side-chains of Asp-96 and Thr-46, and as the cluster grows, it reaches the retinal during the M to N reaction (*10*), allowing reprotonation of the Schiff base by Asp-96. The redistribution and entry of water into this region is very likely the consequence of side-chain repacking (*12*) in response to the movements of Lys-216 and Trp-182 upon relaxation of the isomerized retinal into its bent shape. The observation that small cavities are formed before the N state had already suggested (*10*) that the chain of water molecules between Asp-96 and the retinal is created by the gradual opening of the cavities and the recruitment of water by wat502 to fill them.

The understanding of how the Schiff base is reprotonated in the M to N reaction has been aided considerably by studies (*28*−*31*) of the photocycles of mutants of Asp-96. The replacement of Asp-96 with a non-ionizable residue, such as Gly, Ala, or Asn, removes the internal proton donor. Reprotonation of the Schiff base becomes pH dependent, suggesting that the proton is taken up from the bulk. The change of the volume of the side-chain may be expected to alter the distribution of water nearby and, thereby, the conduction of the proton to the Schiff base. The possibility cannot be excluded that the phenotypes depend not only on the removal of Asp-96 but also on the kind of side-chain that replaced it. Indeed, the observations that the decay of M is much slower (*20*, *31*) in D96N than in D96A and D96G and that azide, a weak acid, strongly accelerates the reprotonation of the Schiff base in the D96N mutant but not in the wild-type or even in D96A and D96G are hints (*20*) that the proton conduction path in D96N is unique and that it depends on the introduced asparagine. This idea is supported by the crystallographic structure of this mutant (*13*). In D96N, the hydrogen bond between the side chains of Asp-96 and Thr-46 is removed, and the amide nitrogen of Asn-96 is connected to the Thr via a new water molecule, wat504.

These observations had suggested that the nature of the side chain of residue 96 might have influence on the distribution of water molecules in the cytoplasmic region. Mutations of Asp-96 affect the photocycle not only because this residue is the proton donor to the Schiff base but also because the Asp-96/Thr-46 pair will organize the pathway for proton conduction. We report here on the crystallographic structures of the non-illuminated and M states in the D96A mutant and compare them to the non-illuminated states of the T46V and the wild type protein, and the M state of D96N. The results indicate that changes of the sidechain of residue 96 have consequences that are not only local but also communicated to other locations including the extracellular region through atomic displacement along a track comprised of Thr-46, wat502, and Lys-216 and result in the redistribution of bound water throughout the protein. This track also appears to function in the photocycle. In contrast to D96A, no such cascade of changes is observed in the less perturbed T46V mutant.

EXPERIMENTAL PROCEDURES

The bacteriorhodopsin crystals, grown in cubic lipid phase as described (*32*), were thin hexagonal plates about 120 μm $\times$ 120 μm $\times$ 10−15 μm. Pieces of the cubic phase with encased crystals were soaked overnight in the mother liqueur plus 0.5% octylglucoside[1], and the crystals were removed and mounted by mechanical manipulation with a nylon loop.

Diffraction data were collected at 100 K from either non-illuminated crystals, or after illumination for 3 s at room temperature and rapid cooling with a cold nitrogen stream to 100 K. Illumination was with a 5 mW He-Ne laser at 628 nm. The diffraction measurements were taken at beamlines BL 9-1 and 11-1 of SSRL (Stanford, California), using a 3 $\times$ 3 array CCD detector (ADSC, San Diego). For each data set, 90 images with a 1° oscillation angle were collected, integrated, and scaled with HKL2000 (*33*), in the $P6_3$ space group, with minor variations from $a = 61$ Å, $b = 61$ Å, $c = 108$ Å, and $\alpha = 90°$, $\beta = 90°$, and $\gamma = 120°$.

Refinement of models was performed with SHELXL-97, as before (*34*), but with single conformations because occupancy of the desired state (non-illuminated or M) was essentially 100%. The input model was first 1C3W to produce omit maps that contained evidence for the replaced side-chains, and then with Asp-96 replaced with Ala or Thr-46 replaced with Val. Superimposition of coordinate sets for calculating displacements of selected atoms was with the program package CCP4i. Cavities were calculated with Molsoft ICM version 3.4-5 (Molsoft L.L.C. La Jolla, CA). The coordinates and the diffraction data for the non-illuminated states of D96A and T46V and the M state of D96A are deposited at the Protein Data Bank with accession codes 2I1X, 2I22, and 2I20, respectively.

RESULTS AND DISCUSSION

In the following, we examine specific structural features of wild-type bacteriorhodopsin and the D96A and T46V mutants. In such comparisons, if the differences in the atomic positions or the cavity sizes are real, then they must exceed the magnitude of positional error between different crystals of the same kind. For the wild-type, this variability was estimated from the averages and standard deviations in independent models refined from diffraction data from five crystals, with resolutions ranging from 1.43 to 1.60 Å. Two of these are published, alone or as part of a determination of a photocycle intermediate (*35*, *36*), but three are from newly collected data. For the T46V mutant, the positional

[1] Abbreviation: octylglucoside, *n*-octyl-β-D-glucopyranoside.

Table 1: X-ray Data Collection and Refinement Statistics for Data Sets from a Non-Illuminated and an Illuminated Crystal of the D96A Bacteriorhodopsin Mutant[a]

	non-illuminated D96A	illuminated D96A	non-illuminated T46V
data resolution range, Å	2.0−25.0	2.08−25.0	1.84−25.0
total observations	306,070	207,357	356,040
unique reflections	15,618	13,966	19,393
R_{merge}[b,d], %	6.2 (75.6)	6.6 (62.5)	4.1 (53.7)
average $I/\sigma(I)$[c,d]	23.4 (2.9)	23.4 (3.8)	28.9 (2.1)
completeness[d], %	99.9 (99.9)	100.0 (100.0)	95.5 (90.5)
mosaicity, °	0.57	0.61	0.84
refinement range, Å	2.0−25.0	2.08−25.0	1.84−25.0
structure factors	14,807	13,226	18,360
restraints	8,206	8,240	8,223
parameters	8,284	8,272	8,300
twin ratio	97:3	58:42	99:1
protein atoms	1717	1717	1720
retinal atoms	20	20	20
water molecules	23	23	24
lipid atoms	310	310	310
R-factor[e,f], %	23.9 (19.8)	15.6 (15.3)	19.5 (17.2)
R_{free}[f,g], %	29.9 (25.9)	26.0 (23.7)	26.0 (23.2)
average protein B, Å^2	32.0	29.2	30.9
average retinal B, Å^2	25.0	22.7	20.5
average water B, Å^2	38.3	39.5	34.0
average lipid B, Å^2	68.5	71.1	72.6
deviation from ideal bond lengths, Å	0.015	0.015	0.015
deviation from ideal bond angle distances, Å	0.054	0.055	0.054

[a] The illumination at 295 K with a red laser, as described in Experimental Procedures, converted bacteriorhodopsin in the crystal to the M state with virtually full occupancy. [b] $R_{merge}(I) = \Sigma_{hkl}\Sigma_i |I_{hkl,i} - \langle I_{hkl}\rangle|/\Sigma_{hkl}\Sigma_i |I_{hkl,i}|$, where $\langle I_{hkl}\rangle$ is the average intensity of the multiple $I_{hkl,i}$ observations for symmetry-related reflections. [c] $I/\sigma(I)$, average of the diffraction intensities divided by their standard deviations. [d] The values in parentheses are for the 2.00 to 2.09 Å and the 2.08 to 2.17 Å shell resolution shells for the non-illuminated and the illuminated D96A crystal, respectively, and the 1.84 to 1.92 Å shell resolution shell for the T46V crystal. [e] *R*-factor $= \Sigma_{hkl}|F_{obs} - F_{calc}|/\Sigma_{hkl}|F_{obs}|$, where F_{obs} and F_{calc} are observed and calculated structure factors, respectively. [f] The values are for all data,with those in parentheses for $F > 4\sigma(F)$. [g] $R_{free} = \Sigma_{hkl} \epsilon T|F_{obs} - F_{calc}|/\Sigma_{hkl} \epsilon T|F_{obs}$, where a test set (5% of the data) is omitted from the refinement in such a way that all structure factors in each of several thin resolution-shells were selected to avoid bias from merohedral twinning.

errors are calculated from models for four crystals, with resolutions between 1.84 and 1.92 Å. The crystallographic resolution for D96A is 2.0 Å (two crystals). There was no detectable twinning in the crystals of the two mutants, that is, the quality of the data is more or less equivalent to that of the wild type. The statistics for the data and the refinement of models for the D96A and T46V mutants are given in Table 1. The standard deviations for interatomic distances in the five wild-type models will be given in the comparisons below and are ± 0.06−0.20 Å depending on the location, in line with earlier attempts to determine crystal-to-crystal reproducibility in our bacteriorhodopsin crystals (*37*). When we conclude that the structural feature is different, it is only when the change of interatomic distance or cavity size is well above the corresponding standard deviation (or in the case of D96A, the range from two independent crystals).

Our intent was to also compare the structural changes in the M (last M substate, or M_2') states produced by the illumination of the D96A and D96N mutants under the same conditions, that is, at ambient temperature. Although it would be more relevant for the transport function to use the M state of the wild-type as reference, this is not possible. In the wild-type protein, M decays too rapidly at room temperature to accumulate in amounts more than a few percent under usual illumination conditions. To populate this state, in the two studies of wild-type M produced in cubic phase grown crystals at ambient temperature (*10*, *38*), the illumination was continued for a short time (1 s) as the crystals were rapidly cooled, and thus, the M was produced at some undefined temperature below the ambient temperature. Such a regime produces either a claimed mixture (*38*) of early and late M, or in our experience (*10*), an M state earlier than M_2'. In both cases, the retinal assumed configurations different from those in M of D96N. In two other studies, the illumination of the crystals was at 210 K (*36*) and 230 K (*40*), and the M produced was also an earlier M, that is, M_1, with fewer changes than those of the later M states. In yet another study of the wild-type M intermediate, with crystals of a different kind where the crystal contacts were suggested to slow the decay of M and allow its accumulation at ambient temperature (*41*), the structural changes do not seem to be comparable to those in cubic phase crystals. In this case, there was virtually no change from the BR state near residue 96, where our attention is focused, but a sliding movement of helix G not seen in the other M structures was reported. The M state of the E204Q mutant (*12*), however, shows similarities to the structure of the M intermediate of D96N. Although the M produced is an earlier sub-state because the E204Q mutation blocks proton release to the extracellular surface, that is, the $M_2 \rightarrow M_2'$ reaction (*6*), the illumination conditions are most similar to those used for the D96A and D96N mutants.

Because the illuminated crystals contained little of the non-illuminated state of the protein, both models for M, from D96A in this study and from D96N earlier (*13*), are the results of refinements from data with full occupancy. The resolution of the data for M of D96N was 2.0 Å, and for D96A it is 2.08 Å (the latter from a crystal with merohedral twinning (see Table 1), as in the earlier report).

Structural Changes in the Non-Illuminated State from Replacement of Asp-96. The crystal structure of the non-illuminated F219L mutant had revealed (*10*) that the cavity created by the side-chain replacement is filled by two water molecules hydrogen bonded to each other and to an existing water (wat501). Comparison of the $2F_{obs} - F_{calc}$ electron density maps of the immediate neighborhood of residue 96 in the D96A mutant and the wild type (Figure 1a and b) shows, however, that this is not always the case. The cavity between Ala-96 and Thr-46 from the smaller Ala side-chain, with a volume of 23−25 Å^3, contains no density. As in the wild type, the side chain of Thr-46 donates a hydrogen bond to the peptide C═O of Phe-42 (not shown in Figure 1), but the energy penalty of inserting a water molecule into this low-dielectric matrix is evidently not compensated by the hydrogen bond this water would donate to OG1 of Thr-46. In contrast, the replacement of the protonated carboxyl of

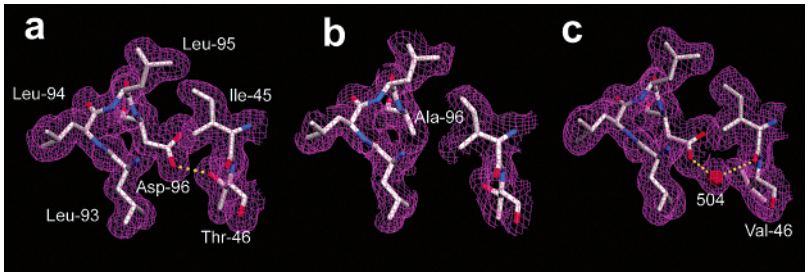

FIGURE 1: Electron density ($2F_{obs} - F_{calc}$) maps of the Asp-96 region in the non-illuminated state in wild-type bacteriorhodopsin (a), the D96A mutant (b), and in T46V (c). Contour level at 1 σ. The wild-type model and map are from 1C3W (*32*).

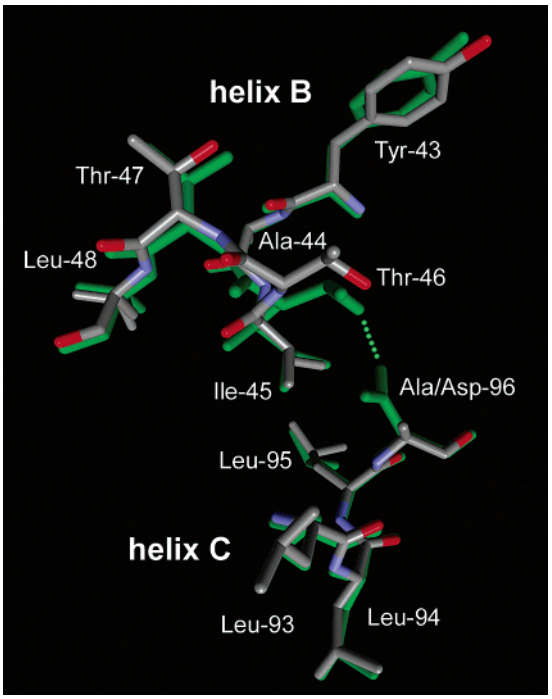

FIGURE 2: Comparison of the Asp-96/Thr-46 region that connects helices B and C in the non-illuminated states in D96A and the wild type. The model for the mutant is shown with atomic colors, and the wild-type model (*32*) is in green.

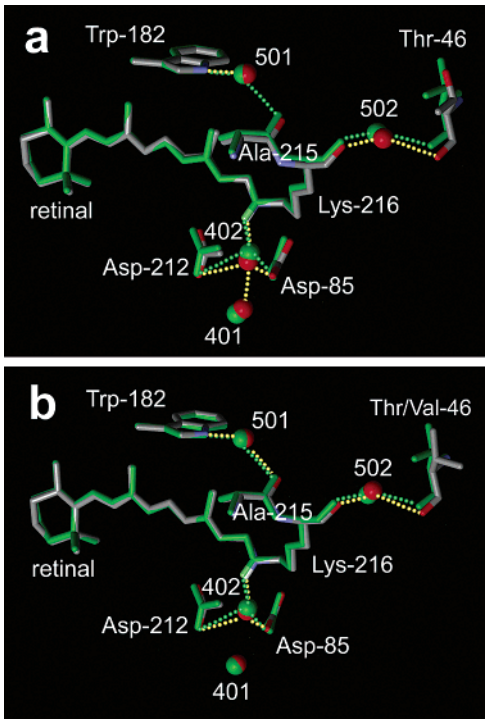

FIGURE 3: Comparison of the retinal region of the non-illuminated states of the D96A (a) and T46V (b) mutants (shown with atomic colors) with that of the wild type (*32*) (in green).

residue 96 with an amide in D96N causes (*13*) an insertion of a water molecule to bridge the amide ND2 and OG1 of Thr-46, and creates no cavity.

The Asp to Ala residue replacement in D96A, and the consequent loss of the hydrogen bond between Asp-96 and Thr-46 that connects helices B and C, will perturb this region. As shown in Figure 2, where the model of D96A is overlaid on the wild-type structure (latter in green), the cytoplasmic ends of helices B and C move apart. As a result, the distance between CA atoms of residue 96 and Thr-46 increases by nearly 1 Å. Another indication of perturbation is the increase of a small cavity in the protein, bound by helices B, C, and G, that extends from the Thr-46 region toward the retinal (not shown). In the wild type, this cavity has a volume of 75 ± 4 Å^3, but in D96A, it nearly doubles in size to 136−143 Å^3. Otherwise, the main-chain and side-chain displacements from the D96A mutation are local, however, and do not extend significantly toward the center of the protein beyond Leu-48 on helix B and Leu-93 on helix C (Figure 2).

Although the primary main-chain and side-chain perturbations from the D96A mutation in Figure 2 do not reach the retinal region, water molecules are affected as far away as the Schiff base and beyond, that is, at a distance as far as 15 Å. Because these water molecules form hydrogen bonds with functionally important residues and play prominent roles in the proton transport mechanism (*42*, *43*), their displacements may be meaningful.

We had suggested earlier that the retinal region is connected to the Asp-96/Thr-46 region through a continuous chain of covalent and hydrogen bonds that appear to have a functional role during the photocycle (*12*). The structure of the D96A mutant (atomic color model in Figure 3a) reveals that the retinal Schiff base region is influenced by the displacement of Thr-46 via the same chain. In the wild type, wat501 bridges helices G and F through hydrogen bonds to the peptide O of Ala-215 and NH1 of Trp-182 (green model in Figure 3a). The hydrogen bond of wat501 to Trp-182 is essentially unchanged in the D96A mutant (its length is 2.91 − 3.05 Å vs 2.80 ± 0.06 Å in the wild type). However, the hydrogen-bond between wat501 and the O of Ala-215 is broken as the interatomic distance increases from 2.97 ± 0.07 Å in the wild type to 3.30−3.52 Å. This appears to be an indirect consequence of the displacement of helix B at Thr-46 as follows. Wat502 moves with the movement of Thr-46 described above because its hydrogen bonds with the

peptide O of Thr-46 (2.87−3.00 Å vs 2.95 ± 0.09 Å in the wild type) and with the peptide O of Lys-216 also (2.94−2.95 Å vs 3.02 ± 0.12 Å in the wild type) are maintained (Figure 3a). Ala-215 is linked to the cytoplasmic region via the hydrogen bond of the peptide O of Lys-216 to wat502. Displacement of wat502, therefore, causes the main chain of helix G to move at Lys-216 and Ala-215, and the peptide O of Ala-215 moves away from wat501, its hydrogen-bonding partner in the wild-type protein.

Unexpectedly, as shown in Figure 3a, water molecules are displaced in the D96A mutant also in the extracellular region. Wat402 is coordinated by the Schiff base nitrogen (NZ of Lys-216) and the OD2 of two anionic residues, Asp-85 and Asp-212. Wat402 is displaced strongly toward Asp-85 (the length of its hydrogen bond with OD2 of Asp-85 is 2.30−2.46 Å vs 2.67 ± 0.13 Å in the wild type), whereas its distance to Asp-212 is nearly unaffected (2.99−3.30 Å vs 3.04 ± 0.20 Å in the wild type). Surprisingly, in the D96A mutant, wat401, the link of Asp-85 to the extracellular aqueous network, moves close enough to wat402 to form a new hydrogen bond (interwater distance is decreased from 3.68 ± 0.17 Å in the wild type to 2.87−3.06 Å). The approach of wat401 and wat402 is partly from the displacement of wat402 but mostly from the movement of wat401 (Figure 3a). In spite of this movement, the hydrogen bonds of wat401 to its partners in the wild type (Asp-85 and wat406) are relatively unaffected (not shown in Figure 3a). Likewise, although there is minor redistribution of the side chains in the extracellular region, no hydrogen bonds are broken or formed as a result of the movement of wat401.

The observed movements of protein atoms, and particularly water far from the site of the D96A mutation, urge caution in interpreting the phenotypes of all mutations in terms of local effects and in assigning O−H bands to specific water molecules solely on the basis of the location of mutations that affect them.

Little of this cascade of displacements between Thr-46 and the retinal region is evident in the earlier determined structure (*13*) of the more conservative mutant, D96N. The chain of hydrogen bonds through O of Thr-46, wat502, and O of Lys-216 is unaffected by the smaller movement of helix C in this mutant, and the hydrogen bond between O of Ala-215 and wat501 is not broken (not shown). The cytoplasmic cavity between Thr-46 and the retinal is only slightly increased, if at all, relative to that of the wild type (to 82 Å^3 vs 75 ± 4 Å). The changes in the extracellular region are also less in D96N. Thus, although wat402 moves closer to the OD2 of Asp-85 in D96N (2.30 Å vs 2.67 ± 0.13 Å in the wild type) as in D96A, the interatomic distance between wat401 and wat402 is decreased (to 3.36 Å vs 3.68 ± 0.17 Å in the wild type) but not sufficiently to form a hydrogen bond.

Structural Changes in the Non-Illuminated State from Replacement of Thr-46. The Thr-to-Val change for residue 46 breaks its hydrogen bond with Asp-96 as does the D96A mutation, but there are two important differences. First, the side-chain is replaced without change of volume. Second, the energy penalty of burying the highly polar COOH of residue 96 without a hydrogen-bonding partner in T46V must be greater than burying the OH of the Thr in D96A. Indeed, the $2F_{obs} - F_{calc}$ electron density map in this region is different in the T46V and the D96A mutants (compare Figure 1b and c). There is no new cavity at residue 96 as in D96A, because a new water molecule, wat504, intercalates and forms a hydrogen bond with the OD2 of Asp-96 and O of Ile-45.

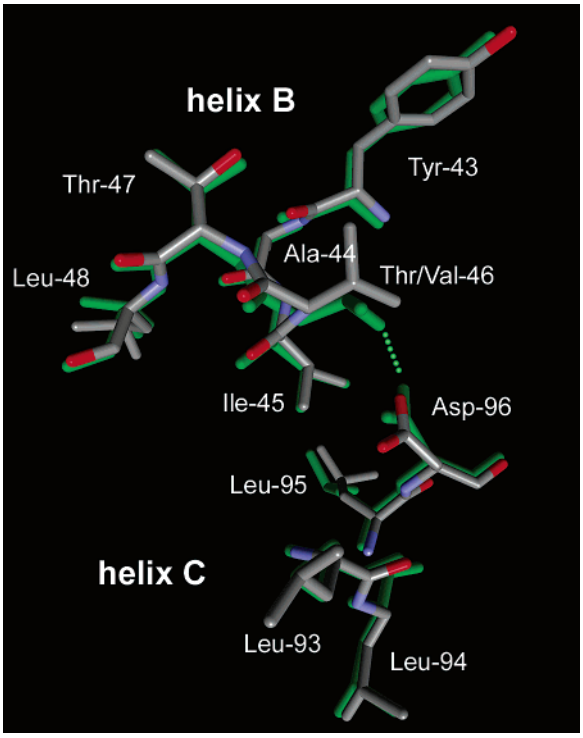

FIGURE 4: Comparison of the Asp-96/Thr-46 region that connects helices B and C in the non-illuminated states in T46V and the wild type. The model for the mutant is shown with atomic colors, and the wild-type model (*32*) is in green.

Consistent with the absence of a cavity at residue 96 and the formation of a new hydrogen bond that retains the link between helices B and C, the perturbation of the Asp-96 region in the T46V mutant is less than that in D96A (Figure 4). The distance between the CA atoms of Asp-96 and residue 46 is increased by less than 0.5 Å relative to that of the wild type, and this change is from the movement of both residues rather than mainly from Thr-46 as in D96A (Figure 2). The cavity that extends toward retinal is increased in size but less than that in D96A, from 75 ± 4 Å^3 in the wild type to 94 ± 5 Å^3. As in the D96A mutant, the perturbation is local, and little change is observed a few residues away on either helix B or C (Figure 4).

Consistent with the smaller perturbation at residue 46, the retinal region is less affected. As shown in Figure 3b, the hydrogen bond of Ala-215 with wat501 is maintained (interatomic distance 2.97 ± 0.06 Å). Wat401 does not move significantly, and a new hydrogen bond between wat402 and wat401 is not formed (interatomic distance 3.41 ± 0.09 Å).

In an earlier study of 2D crystals of the T46V mutant (*17*), a density feature at helix C was observed in the non-illuminated T46V versus the non-illuminated wild-type difference projection map. Its origin may well be the separation of helices B and C in Figure 4.

Structural Changes in the M State from the Replacement of Asp-96. Given the structural changes in the non-illuminated D96A mutant described above, it would be informative to know how they affect the structure of the M state. The decay of the M state is greatly slowed by the

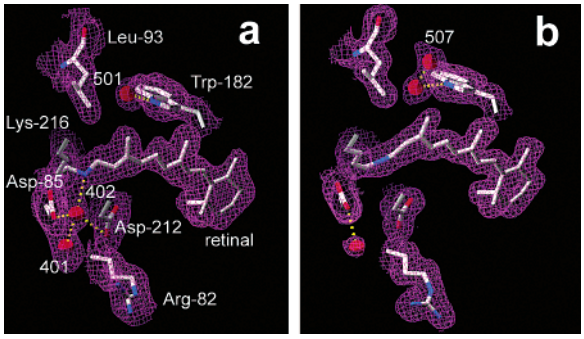

FIGURE 5: Electron density ($2F_{obs} - F_{calc}$) maps of the retinal region in the non-illuminated state (a) and the trapped M state (b) in the D96A mutant. Contour level at 1 σ.

replacement of Asp-96 with a non-protonatable residue, particularly at higher pH (*31*−*34*), and this allows accumulation of the last M state (M_2') in a photostationary state. Indeed, as with the D96N crystals at neutral pH (*13*), a full color change from purple to yellow upon illumination of D96A crystals at pH 8.5 at ambient temperature indicated the virtually complete conversion to the M state. This state was then trapped by rapidly dropping the temperature to 100 K, as before (*13*).

Figure 5a and b compare $2F_{obs} - F_{calc}$ electron density maps of the non-illuminated and M states of D96A, respectively. As expected, the trapped M state of this mutant bears considerable similarity to the earlier reported (*13*) M of D96N: the retinal is 13-cis,15-anti, wat402 and wat406 are absent in the map (latter not shown), wat401 forms a hydrogen-bond with OD2 of Asp-85, and the Arg-82 side-chain is rotated toward the extracellular surface. An unexpected feature in M is a new water molecule, wat507, hydrogen bonded to wat501. A water molecule had been reported (*13*) at this location in the non-illuminated, although not in the M state, of D96N.

Elsewhere in the protein, however, the M states of D96A and D96N are different. Figure 6a and b shows models of the retinal region in the M states (atomic colors) of D96N and D96A, respectively, each superimposed on the non-illuminated state of the same mutant (blue color). In D96N (Figure 6a), the rotation of the retinal C_{15}=NZ-CE segment with the deprotonated Schiff base from the extracellular to the cytoplasmic direction and the accompanying changes of the geometry of the retinal polyene chain and the Lys-216 side chain move the main chain of helix G at Lys-216 and, therefore, at Ala-215 (for a detailed discussion of this, see refs 12 and 13 (*12*, *13*)). The displacement of the O of Ala-215 breaks its hydrogen bond with wat501, and there is no electron density for this water in M. The connection of helix G to helix F through this water and Trp-182 is, thereby, eliminated, and the Trp ring is free to tip upward from the approach of the 13-methyl group of the retinal (Figure 6a). The movement of Lys-216 moves the connected wat502 and the O of Thr-46, moving OG1 of Thr-46 away from Asn-96. Inasmuch as the same kinds of changes occur at these locations in the trapped M state of the E204Q mutant (*12*), this structural shift may occur in the wild-type M as well. It should have the rationale to lower the pK_a of Asp-96; therefore, it will become the proton donor to the Schiff base.

The displacements of Ala-215, Lys-216, wat502, and wat401 (but not Trp-182, and obviously not the retinal) in

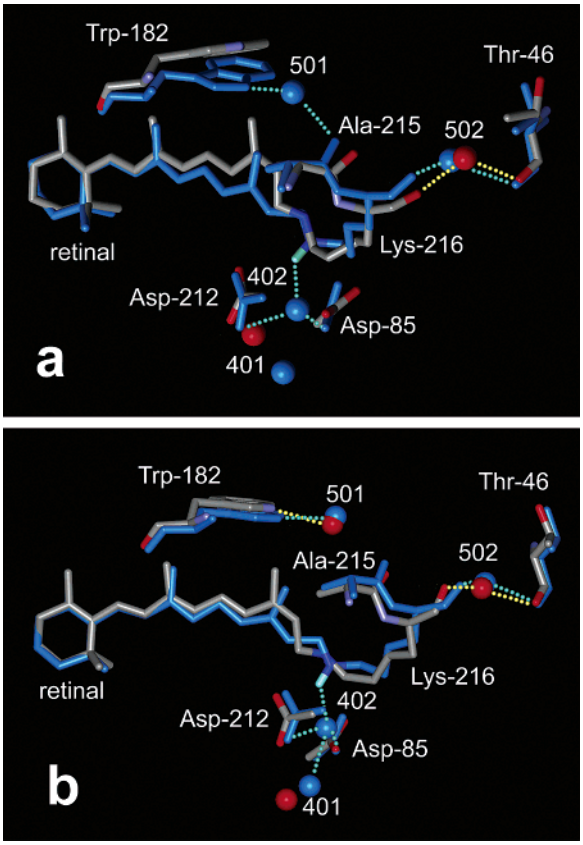

FIGURE 6: Comparison of the retinal region of the trapped M states of the D96N (*13*) (a) and D96A (b) mutants (shown with atomic colors) with their respective non-illuminated states (in blue).

the M of D96N (Figure 6a) are similar to those in the non-illuminated state of the D96A mutant (Figure 3a), although they are greater in magnitude. Thus, in both models, the O of Ala-215 moves away from wat501, wat502 is moved by the displacement of Lys-216, and wat401 approaches the two aspartate carboxyls. In the M state, the perturbation originates at the retinal and spreads to Asn-96 via Thr-46 (Figure 3a), whereas in D96A, the perturbation originates at residue 96 and spreads to Thr-46 and then the retinal region (Figure 6a). It appears that the same track of covalent and hydrogen-bonds can be the means for propagating structural perturbation in both directions.

The changes in the position of Ala-215, wat502, and wat401 in M of D96N will have already partly occurred in the non-illuminated D96A. Consistent with the perturbation of this region, although the movements of the retinal in the M state of D96A (Figure 6b) are similar to those of the M state of D96N (Figure 6a), the ensuing displacements of Lys-216, Ala-215, Lys-216, and wat501 are less extensive. For example, the movement of the O of Ala-215 in the M state of D96N relative to that in the non-illuminated state is 0.97 Å, but in the M state of D96A, it is only 0.55 Å. Water 502, connected to the O of Lys-216, moves by 1.00 Å in the M of D96N but 0.51 Å in the M state of D96A. As a result, in the M state of D96A, communication of the retinal region with the Thr-46 region will have been impaired, and Thr-46 should be less displaced.

Figure 7a and b compares the region of Thr-46 in the non-illuminated and M states, in D96N and D96A, respectively. In the M of D96N, the displacement of wat502 toward O of Thr-46 allows movement of the peptide segment, and the

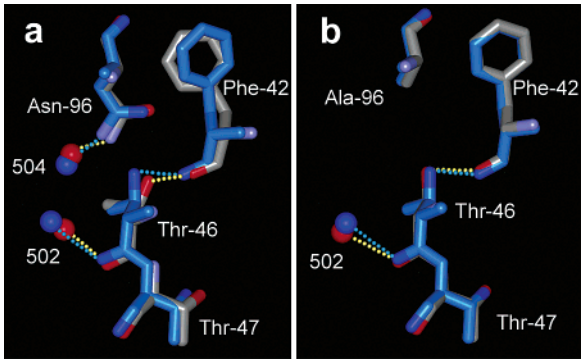

FIGURE 7: Comparison of the Asp-96/Thr-46 region in the trapped M states of the D96N (*13*) (a) and the D96A (b) mutants. The models for M are shown with atomic colors, and the models for their respective non-illuminated states are in blue.

ensuing torsion of the main chain moves OG1 of Thr-46 away from wat504 (by 0.88 Å). The interatomic distance between these atoms increases from 3.29 to 4.02 Å, and the weak hydrogen bond breaks. Because the other hydrogen bonds in this region are maintained, the bulky side chain of Phe-42, a participant of the cytoplasmic hydrophobic barrier (*10*) like Phe-219, moves, presumably in anticipation of the increased hydration that allows conducting a proton to the retinal Schiff base in the next step of the photocycle.

In the M of D96A, the smaller, and more importantly lateral, displacement of wat502 relative to O of Thr-46 results in fewer changes at Thr-46 (Figure 7b). In D96A, OG1 of Thr-46 undergoes virtually no movement in M (its displacement is only 0.14 Å).

In the earlier described trapped M state of D96N, the cytoplasmic ends of helices F and G as well as part of the E−F interhelical loop were too disordered to model (*13*). The disorder along helix F begins at Val-177, which is displaced in a manner consistent with the outward tilt of the cytoplasmic end of helix F detected in many other studies (*16*−*22*). Thus, it may be the result of the tilt that disrupts the crystal locally and as such constitutes evidence for this large-scale conformational shift. However, we detect neither the disorder nor an observable tilt of helix F in the trapped M of D96A, consistent with the lack of structural changes at the Ala-96/Thr-46 pair (Figure 7b). In this respect, the M states of D96A and D96N also seem to differ. Such a difference was reported before. In the projection map of the M state of a 2D crystal of the D96G mutant (*17*), density changes were detected at helices F and G, but the difference map had considerably less magnitude at helix F than that in the M state of the wild type and D96N. The smaller tilt of helix F was attributed to an alteration of conformational flexibility in the D96G mutant but not in the more conservative D96N mutant. This observation and its interpretation are consistent with the 3D structure we report here for the D96A mutant.

CONCLUSIONS

The D96A and the T46V mutations in the cytoplasmic region of bacteriorhodopsin both break the functionally important hydrogen bond between Asp-96 and Thr-46, but in the former mutant, the structural perturbation is greater and propagates to the retinal and the extracellular region by a track of covalent and hydrogen bonds that include wat502, which links helix B to helix G. The same track is utilized in the functional cycle of this proton pump to propagate structural changes from the photoisomerized retinal to Asp-96. If one can generalize from these findings, it seems possible that the structure of well-chosen mutants of bacteriorhodopsin-like heptahelical membrane proteins will reveal the details of functionally relevant conformational changes otherwise difficult to measure.

ACKNOWLEDGMENT

We thank the beamline staff at SSRL for their essential assistance and F. Jurnak and S. Heffron for help with cavity calculations.

REFERENCES

1. Brown, L. S. (2001) Proton transport mechanism of bacteriorhodopsin as revealed by site-specific mutagenesis and protein sequence variability, *Biochemistry (Moscow). 66*, 1249−1255.
2. Butt, H. J., Fendler, K., Bamberg, E., Tittor, J., and Oesterhelt, D. (1989) Aspartic acids 96 and 85 play a central role in the function of bacteriorhodopsin as a proton pump, *EMBO J. 8*, 1657−1663.
3. Mogi, T., Stern, L. J., Marti, T., Chao, B. H., and Khorana, H. G. (1988) Structure-function studies on bacteriorhodopsin. VII. Aspartic acid substitutions affect proton translocation by bacteriorhodopsin, *Proc. Natl. Acad. Sci. U.S.A. 85*, 4148−4152.
4. Rath, P., Krebs, M. P., He, Y., Khorana, H. G., and Rothschild, K. J. (1993) Fourier transform Raman spectroscopy of the bacteriorhodopsin mutant Tyr-185 → Phe: Formation of a stable O-like species during light adaptation and detection of its transient N-like photoproduct, *Biochemistry 32*, 2272−2281.
5. Balashov, S. P., Imasheva, E. S., Ebrey, T. G., Chen, N., Menick, D. R., and Crouch, R. K. (1997) Glutamate-194 to cysteine mutation inhibits fast light-induced proton release in bacteriorhodopsin, *Biochemistry 36*, 8671−8676.
6. Brown, L. S., Sasaki, J., Kandori, H., Maeda, A., Needleman, R., and Lanyi, J. K. (1995) Glutamic acid 204 is the terminal proton release group at the extracellular surface of bacteriorhodopsin, *J. Biol. Chem. 270*, 27122−27126.
7. Richter, H. T., Needleman, R., and Lanyi, J. K. (1996) Perturbed interaction between residues 85 and 204 in Tyr-185 → Phe and Asp-85 → Glu bacteriorhodopsins, *Biophys. J. 71*, 3392−3398.
8. Dioumaev, A. K., Richter, H. T., Brown, L. S., Tanio, M., Tuzi, S., Saito, H., Kimura, Y., Needleman, R., and Lanyi, J. K. (1998) Existence of a proton transfer chain in bacteriorhodopsin: participation of Glu-194 in the release of protons to the extracellular surface, *Biochemistry 37*, 2496−2506.
9. Govindjee, R., Misra, S., Balashov, S. P., Ebrey, T. G., Crouch, R. K., and Menick, D. R. (1996) Arginine-82 regulates the pK_a of the group responsible for the light-driven proton release in bacteriorhodopsin, *Biophys. J. 71*, 1011−1023.
10. Schobert, B., Brown, L. S., and Lanyi, J. K. (2003) Crystallographic structures of the M and N intermediates of bacteriorhodopsin: assembly of a hydrogen-bonded chain of water molecules between Asp96 and the retinal Schiff base, *J. Mol. Biol. 330*, 553−570.
11. Dioumaev, A. K., Brown, L. S., Needleman, R., and Lanyi, J. K. (2001) Coupling of the reisomerization of the retinal, proton uptake, and reprotonation of asp-96 in the N photointermediate of bacteriorhodopsin, *Biochemistry 40*, 11308−11317.
12. Luecke, H., Schobert, B., Richter, H. T., Cartailler, J.-P., Rosengarth, A., Needleman, R., and Lanyi, J. K. (2000) Coupling photoisomerization of the retinal in bacteriorhodopsin to directional transport, *J. Mol. Biol. 300*, 1237−1255.
13. Luecke, H., Schobert, B., Richter, H. T., Cartailler, J. P., and Lanyi, J. K. (1999) Structural changes in bacteriorhodopsin during ion transport at 2 angstrom resolution, *Science 286*, 255−261.
14. Yohannan, S., Yang, D., Faham, S., Boulting, G., Whitelegge, J., and Bowie, J. U. (2004) Proline substitutions are not easily accommodated in a membrane protein, *J. Mol. Biol. 341*, 1−6.
15. Rouhani, S., Cartailler, J. P., Facciotti, M. T., Walian, P., Needleman, R., Lanyi, J. K., Glaeser, R. M., and Luecke, H. (2001) Crystal structure of the D85S mutant of bacteriorhodop-

sin: model of an O-like photocycle intermediate, *J. Mol. Biol. 313*, 615−628.
16. Subramaniam, S., Gerstein, M., Oesterhelt, D., and Henderson, R. (1993) Electron diffraction analysis of structural changes in the photocycle of bacteriorhodopsin, *EMBO J. 12*, 1−8.
17. Subramaniam, S., Lindahl, M., Bullough, P., Faruqi, A. R., Tittor, J., Oesterhelt, D., Brown, L., Lanyi, J., and Henderson, R. (1999) Protein conformational changes in the bacteriorhodopsin photocycle, *J. Mol. Biol. 287*, 145−161.
18. Subramaniam, S., and Henderson, R. (2000) Molecular mechanism of vectorial proton translocation by bacteriorhodopsin, *Nature 406*, 653−657.
19. Dencher, N. A., Dresselhaus, D., Zaccai, G., and Bueldt, G. (1989) Structural changes in bacteriorhodopsin during proton translocation revealed by neutron diffraction, *Proc. Natl. Acad. Sci. U.S.A. 86*, 7876−7879.
20. Kataoka, M., Kamikubo, H., Tokunaga, F., Brown, L. S., Yamazaki, Y., Maeda, A., Sheves, M., Needleman, R., and Lanyi, J. K. (1994) Energy coupling in an ion pump. The reprotonation switch of bacteriorhodopsin, *J. Mol. Biol. 243*, 621−638.
21. Kamikubo, H., Kataoka, M., Varo, G., Oka, T., Tokunaga, F., Needleman, R., and Lanyi, J. K. (1996) Structure of the N intermediate of bacteriorhodopsin revealed by x-ray diffraction, *Proc. Natl. Acad. Sci. U.S.A. 93*, 1386−1390.
22. Kamikubo, H., Oka, T., Imamoto, Y., Tokunaga, F., Lanyi, J. K., Kataoka, M. (1997) The last phase of the reprotonation switch in bacteriorhodopsin: the transition between the M-type and the N-type protein conformation depends on hydration, *Biochemistry 36*, 12282−12287.
23. Brown, L. S., Kamikubo, H., Zimanyi, L., Kataoka, M., Tokunaga, F., Verdegem, P., Lugtenburg, J., and Lanyi, J. K. (1997) A local electrostatic change is the cause of the large-scale protein conformation shift in bacteriorhodopsin, *Proc. Natl. Acad. Sci. U.S.A. 94*, 5040−5044.
24. Thorgeirsson, T. E., Xiao, W., Brown, L. S., Needleman, R., Lanyi, J. K., and Shin, Y. K. (1997) Transient channel-opening in bacteriorhodopsin: an EPR study, *J. Mol. Biol. 273*, 951−957.
25. Wegener, A. A., Chizhov, I., Engelhard, M., and Steinhoff, H. J. (2000) Time-resolved detection of transient movement of helix F in spin-labelled pharaonis sensory rhodopsin II, *J. Mol. Biol. 301*, 881−891.
26. Dioumaev, A. K., Brown, L. S., Needleman, R., and Lanyi, J. K. (1998) Partitioning of free energy gain between the photoisomerized retinal and the protein in bacteriorhodopsin, *Biochemistry 37*, 9889−9893.
27. Lanyi, J. K., and Schobert, B. (2004) Local-global conformational coupling in a heptahelical membrane protein: transport mechanism from crystal structures of the nine states in the bacteriorhodopsin photocycle, *Biochemistry 43*, 3−8.
28. Tittor, J., Soell, C., Oesterhelt, D., Butt, H. J., and Bamberg, E. (1989) A defective proton pump, point-mutated bacteriorhodopsin Asp96 → Asn is fully reactivated by azide, *EMBO J. 8*, 3477−3482.
29. Otto, H., Marti, T., Holz, M., Mogi, T., Lindau, M., Khorana, H. G., and Heyn, M. P. (1989) Aspartic acid-96 is the internal proton donor in the reprotonation of the Schiff base of bacteriorhodopsin, *Proc. Natl. Acad. Sci. U.S.A. 86*, 9228−9232.
30. Cao, Y., Varo, G., Chang, M., Ni, B., Needleman, R., and Lanyi, J. K. (1991) Water is required for proton transfer from aspartate-96 to the bacteriorhodopsin Schiff base, *Biochemistry 30*, 10972−10979.
31. Miller, A., and Oesterhelt, D. (1990) Kinetic optimization of bacteriorhodopsin by aspartic acid 96 as an internal proton donor, *Biochim. Biophys. Acta. 1020*, 57−64.
32. Rummel, G., Hardmeyer, A., Widmer, C., Chiu, M. L., Nollert, P., Locher, K. P., Pedruzzi, I., Landau, E. M., and Rosenbusch, J. P. (1998) Lipidic cubic phases: new matrices for the three-dimensional crystallization of membrane proteins, *J. Struct. Biol. 121*, 82−91.
33. Otwinowski, Z., and Minor, W. (1997) Processing of X-ray diffraction data collected in oscillation mode, *Macromol. Crystallogr., Part A 276*, 307−326.
34. Sheldrick, G. M. S. T. (1997) High resolution refinement, *Methods Enzymol. 277*, 319−343.
35. Luecke, H., Schobert, B., Richter, H. T., Cartailler, J. P., and Lanyi, J. K. (1999) Structure of bacteriorhodopsin at 1.55 Å resolution, *J. Mol. Biol. 291*, 899−911.
36. Schobert, B., Cupp-Vickery, J., Hornak, V., Smith, S., and Lanyi, J. (2002) Crystallographic structure of the K intermediate of bacteriorhodopsin: conservation of free energy after photoisomerization of the retinal, *J. Mol. Biol. 321*, 715−726.
37. Lanyi, J. K., and Schobert, B. (2003) Mechanism of proton transport in bacteriorhodopsin from crystallographic structures of the K, L, M-1, M-2, and M-2′ intermediates of the photocycle, *J. Mol. Biol. 328*, 439−450.
38. Sass, H. J., Buldt, G., Gessenich, R., Hehn, D., Neff, D., Schlesinger, R., Berendzen, J., and Ormos, P. (2000) Structural alterations for proton translocation in the M state of wild-type bacteriorhodopsin, *Nature 406*, 649−653.
39. Lanyi, J. K., and Schobert, B. (2002) Crystallographic structure of the retinal and the protein after deprotonation of the Schiff base: the switch in the bacteriorhodopsin photocycle, *J. Mol. Biol. 321*, 727−737.
40. Facciotti, M. T., Rouhani, S., Burkard, F. T., Betancourt, F. M., Downing, K. H., Rose, R. B., McDermott, G., and Glaeser, R. M. (2001) Structure of an early intermediate in the M-state phase of the bacteriorhodopsin photocycle, *Biophys. J. 81*, 3442−3455.
41. Takeda, K., Matsui, Y., Kamiya, N., Adachi, S., Okumura, H., and Kouyama, T. (2004) Crystal structure of the M intermediate of bacteriorhodopsin: allosteric structural changes mediated by sliding movement of a transmembrane helix, *J. Mol. Biol. 341*, 1023−1037.
42. Maeda, A. (2001) Internal water molecules as mobile polar groups for light-induced proton translocation in bacteriorhodopsin and rhodopsin as studied by difference FTIR spectroscopy, *Biochemistry (Moscow) 66*, 1256−1268.
43. Kandori, H. (2004) Hydration switch model for the proton transfer in the Schiff base region of bacteriorhodopsin, *Biochim. Biophys. Acta. 1658*, 72−79.

BI061310I